Recent results for (e,e'p) reactions at Jefferson Lab

D. Potterveld[1], D. Abbott[21], A. Ahmidouch[7], T. Amatuoni[24], C. Armstrong[23], J. Arrington[2], K. A. Assamagan[6], O. K. Baker[6], S. Barrow[17], K. Beard[6], D. Beatty[17], S. Beedoe[13], E. Beise[11], E. Belz[4], C. Bochna[9], H. Breuer[11], E. E. W. Bruins[10], R. Carlini[21], J. Cha[6], N. Chant[11], C. Cothran[22], W. J. Cummings[1], S. Danagoulian[13], D. Day[22], D. DeSchepper[10], J.-E. Ducret[20], F. Duncan[11], J. Dunne[21], D. Dutta[14], T. Eden[6], R. Ent[21], J. Fedchak[1], H. T. Fortune[17], V. Frolov[18], D. F. Geesaman[1], H. Gao[9], R. Gilman[19], P. Gueye[6], J. O. Hansen[1], W. Hinton[6], R. Holt[9], C. Jackson[13], H. E. Jackson[1], C. Jones[1], S. Kaufman[1], J. J. Kelly[11], C. Keppel[6], M. Khandaker[12], Wooyoung Kim[8], E. Kinney[4], A. Klein[16], D. Koltenuk[17], L. Kramer[10], W. Lorenzon[17], A. Lung[2], K. McFarlane[12], D. Mack[21], R. Madey[6,7], P. Markowitz[5], J. Martin[10], A. Mateos[10], D. Meekins[21], M. Miller[9], R. Milner[10], J. Mitchell[21], H. Mkrtchyan[24], R. Mohring[11], G. Niculescu[6], I. Niculescu[6], T. G. O'Neill[1], J. W. Price[18], J. Reinhold[1], C. Salgado[12], J. P. Schiffer[1], R. E. Segel[14], P. Stoler[18], R. Suleiman[7], V. Tadevosyan[24], L. Tang[6], B. Terburg[9], W. Turchinetz[10], D. van Westrum[4], Pat Welch[15], C. Williamson[10], S. Wood[21], C. Yan[21], Jae-Choon Yang[3], J. Yu[17], B. Zeidman[1], W. Zhao[10], B. Zihlmann[22]

[1] *Argonne National Laboratory, Argonne IL 60439* [2] *California Institute of Technology, Pasadena CA 91125* [3] *Chungnam National University, Taejon Korea* [4] *University of Colorado, Boulder CO 80309* [5] *Florida International University, University Park, FL 33199* [6] *Hampton University, Hampton VA 23668* [7] *Kent State University, Kent OH 44242* [8] *Kyungpook National University, Taegu, South Korea* [9] *University of Illinois, Champaign-Urbana IL 61801* [10] *Massachusetts Institute of Technology, Cambridge MA 02139* [11] *University of Maryland, College Park MD 20742* [12] *Norfolk State University, Norfolk VA 23504* [13] *North Carolina A & T, Greensboro NC 27411* [14] *Northwestern University, Evanston IL 60201* [15] *Oregon State University, Corvallis OR 97331* [16] *Old Dominion University, Norfolk, VA 23529* [17] *University of Pennsylvania, Philiadelphia PA 19104* [18] *Rensselaer Polytechnic Institute, Troy NY 12180* [19] *Rutgers University, New Brunswick NJ 08903* [20] *CE Saclay, Gif-sur-Yvette France* [21] *Thomas Jefferson National Accelerator Facility, Newport News VA 23606* [22] *University of Virginia, Charlottesville VA 22901* [23] *William and Mary, Williamsburg, VA 23187* [24] *Yerevan Physics Institute, Yeravan, Armenia*

Coincidence cross sections for $(e,e'p)$ quasi-elastic scattering were measured at CEBAF with high statistical precision for C, Fe, and Au targets for $0.6 < Q^2 < 3.3$ GeV^2. Missing energy and missing momentum distributions obtained from a preliminary analysis are in reasonable agreement with prior data from SLAC. The preliminary results are compared with a PWIA calculation to determine the nuclear transparency as a function of Q^2 and A. A Rosenbluth analysis to extract the longitudinal and transverse cross sections from these data is anticipated.

DISCLAIMER

1 Introduction

The elastic scattering of electrons by a free proton is a well understood process, characterized by two electromagnetic form factors in the absence of polarization. When the scattering occurs from a nucleus, the process is more complex. The dominant reaction mechanism at modest Q^2 for kinematics near that of elastic proton scattering is quasi-elastic scattering, in which the electron scatters elastically from a moving, off-shell proton.[1] In the PWIA approximation, the cross section for this mechanism may be written as:

$$\frac{d^6\sigma}{dk'\,dE'_p\,d\Omega_{k'}\,d\Omega_{P'}} = P'\,E'_p\,\sigma_{ep}\,S(E,\vec{P}) \tag{1}$$

where k' is the momentum of the scattered electron, P' and E'_p are the momentum and energy of the scattered proton, σ_{ep} is the elementary electron-proton cross section, and $S(E,\vec{P})$ is the probability density for striking a proton with initial energy E and momentum $\vec{P}$. The spectral function S is directly related to the nuclear wave function, and has normalization:

$$\int S(E,\vec{P})\,d^3\vec{P}\,dE = Z. \tag{2}$$

An exclusive cross section measurement, in which E and P can be (approximately) determined from the final-state kinematics, can thus probe nuclear structure through the spectral function. Complicating this simple picture are effects beyond the PWIA, such as photon radiation, re-interaction of the emerging proton with the A-1 nucleons, and meson exchange currents. Exclusive measurements offer an opportunity to study these effects as well.

Previous work at SLAC[2] and BATES[3] focused on studying the transparency of the residual nucleons to the emerging proton. The SLAC data were compared with theoretical cross sections based on a spectral function derived from an independent particle shell model (IPSM) and including radiative effects and some corrections for short-range correlations in the nuclear wave function.[4] The ratios of experimental to theoretical cross sections $T = \sigma_{\rm exp}/\sigma_{\rm pwia}$ are plotted in Fig. 1. The BATES data were divided by the inclusive cross section after subtraction of the inelastic contribution; these ratios are also plotted in Fig. 1.

Absorption of the scattered protons results in $T < 1$. The ratio decreases with increasing A as one would expect. For $0.3 < Q^2 < 3.0$ GeV^2, T falls with increasing Q^2. This is consistent with the strong energy-dependence of the total proton-nucleon cross section for proton momenta below 1.5 GeV/c. Various authors[5,6,7,8,9,10,11] have attempted to calculate the Q^2 and A dependence of

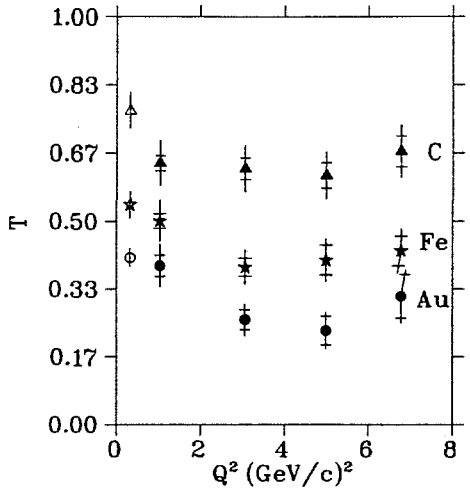

Figure 1: Transparency ratios for $(e, e'p)$ quasi-elastic scattering from C, Fe, and Au targets. The solid data points are the ratio of experimental to PWIA cross sections from Ref. 2. The open points are the ratio of exclusive to inclusive cross sections from Ref. 3. Statistical errors are indicated by horizontal ticks on the total error bars.

these data using a Glauber model of the proton absorption, or including more speculative effects such as color transparency—a proposed reduction in the final state interactions after a hard scattering that would cause an enhancement of the nuclear transparency at high Q^2. The SLAC data are consistent with some Glauber calculations, but cannot rule out the color transparency effect if its onset is slow enough in this kinematic range.

The present experiment studies proton propagation through nuclei in the Q^2 range $0.6 < Q^2 < 3.3$ $(\mathrm{GeV/c})^2$. This is the region where the nuclear transparency is changing rapidly with Q^2, and any color transparency effect is expected to be small. By measuring high statistics data, including backward and forward electron angle data at the same Q^2 to separate the longitudinal and transverse response, we hope to improve our understanding of proton-nucleon interactions and to test the validity of the quasi-elastic reaction mechanism.

2 Experiment

This experiment (E91-013) was performed at CEBAF[a] in Hall C, using the High Momentum (HMS) and Short Orbit (SOS) spectrometers. A 20 μA

[a]Now the Thomas Jefferson National Accelerator Facility.

Table 1: Summary of measurements. The conjugate proton angles for elastic (e, p) scattering are shown in boldface.

Proton Kinetic Energy (MeV)	Electron Energy (MeV)	Electron Angle (degrees)	Proton Angles (degrees)	Q^2 $(\mathrm{GeV/c})^2$
350	845	78.5	27.8, **31.8**, 35.8, 39.8 43.8, 47.8	0.643
350	2445	20.5	35.4, 39.4, 43.4, 47.4 51.4, **55.4**, 59.4, 63.4 67.4, 71.4, 75.4	0.643
700	2445	32.0	31.0, 35.0, 39.0, **43.0** 47.0, 51.0, 55.0	1.283
970*	1645	80.0	**22.8**, 26.8, 30.8, 34.8	1.781
970	3245	28.6	33.5, 37.5, **40.5**, 44.5, 48.5, 52.5	1.784
1800	3245	50.0	**25.1**, 27.6, 30.1	3.305

* Only C and Fe data for these kinematics.

continuous (CW) beam of electrons was incident on solid targets of C, Fe, and Au, as well as a target of CH_2 plastic and an extended target of liquid hydrogen to check the absolute normalization relative to the well-known *ep* elastic cross section. Table 1 summarizes the measurements made. For each electron angle, cross sections were measured for a range of proton angles spanning the quasi-elastic peak. The HMS was used to detect the scattered electrons and the SOS was used to detect the scattered protons in coincidence, except for the data at a proton kinetic energy of 1.8 GeV, where the spectrometer roles were reversed. Typically, enough data were taken to ensure statistical uncertainties in the cross section of 1% or better.

The SOS consists of a quadrupole magnet followed by two dipoles in a configuration modelled after the MRS spectrometer of LAMPF. It features a short flight path (7.3 m) with large angular acceptance (7.7 msr) and momentum bite (40%), good momentum resolution (0.1%), and a maximum central momentum of 1.7 GeV. The HMS consists of three quadrupoles followed by a dipole, all superconducting with cold iron poles. It has a long flight path (23.2 m), comparable solid angle (6.8 msr), smaller momentum bite (18%), but better momentum resolution (0.05-0.1%), with a maximum central momentum of 7 GeV.

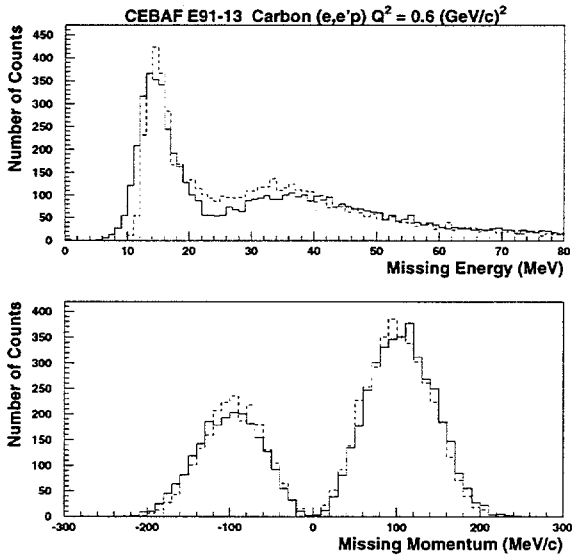

Figure 2: E_m and P_m distributions, not corrected for spectrometer acceptance.

In each spectrometer, four segmented planes of plastic scintillator were used to form a trigger and to provide time-of-flight particle identification. Two 6-plane drift chambers were used to measure the particle trajectories from which the scattering angle and momentum of the particle were calculated. Additional particle identification was provided by a gas threshold Cerenkov detector and a segmented lead glass shower array.

The solid angle of each spectrometer was defined by a 2-inch thick tungsten collimator with a large octagonal hole. These could be exchanged remotely with collimators featuring a grid of small holes. Extensive optics data were taken with these 'sieve-slit' collimators to calibrate the trajectory reconstruction coefficients for the scattering angles. Momentum reconstruction coefficients were determined by observing electrons scattered elastically from C and H nuclei at several spectrometer excitations.

Coincidence triggers were read out through fastbus hardware by the CODA data acquisition system.[12] After time-of-flight corrections, the coincidence timing resolution was typically 0.5 ns (fwhm), with a real to random ratio greater than 200. The calculation of absolute cross sections included corrections for

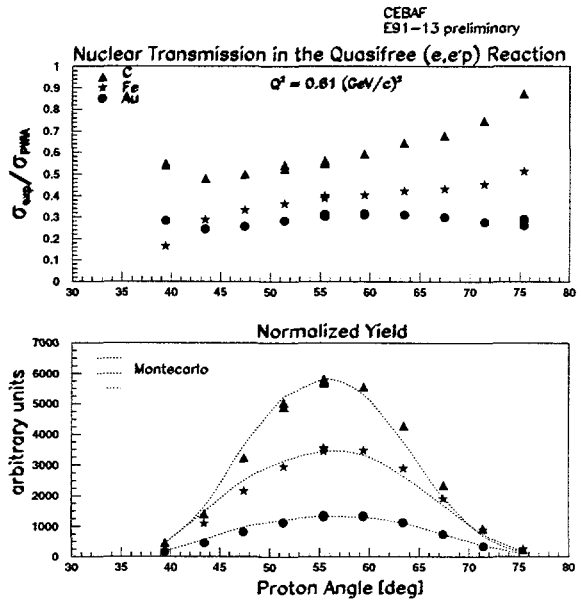

Figure 3: $T = \sigma_{\rm exp}/\sigma_{\rm pwia}$ for $(e, e'p)$ quasi-elastic scattering from C, Fe, and Au targets at $Q^2 = 0.6$ GeV^2, and the yield versus proton angle. The PWIA-based Monte Carlo results are shown as the dotted lines.

detector inefficiencies, computer dead-time, and proton losses from secondary scattering in the target and the spectrometer windows.

3 Preliminary results

The missing energy (E_m) and missing momentum (P_m) are defined as the difference between initial state and observed final-state quantities:

$$\begin{aligned} |P_m| &= |\vec{Q} - \vec{P'}| \\ E_m &= \omega - E'_p + M_p - T_{\rm A-1} \end{aligned} \tag{3}$$

in which $\vec{Q}$ is the 3-momentum transfer, ω is the energy transfer, M_p is the proton mass, and T_{A-1} is the kinetic energy of the A-1 nucleons, with the convention that P_m is positive (negative) if $\vec{P'}$ is at a larger (smaller) angle with respect to the incident electron than $\vec{Q}$. E_m and P_m may be calculated

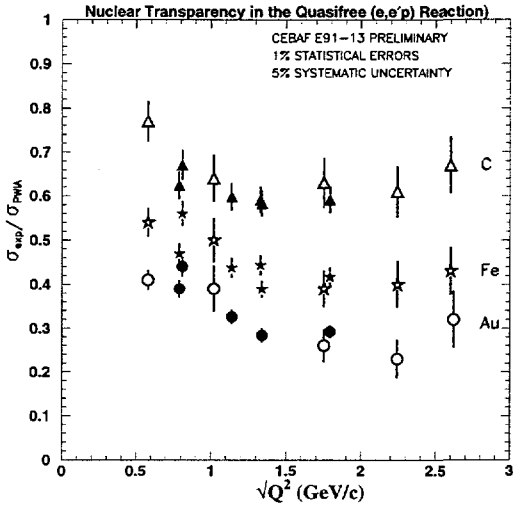

Figure 4: $T = \sigma_{\rm exp}/\sigma_{\rm pwia}$ for $(e,e'p)$ quasi-elastic scattering from C, Fe, and Au targets. Prior data[2,3] is shown as open symbols, and this experiment as solid symbols. The data points at $Q^2 = 0.6$ and $Q^2 = 1.8$ have been displaced sideways slightly to distinguish the error bars.

from the observed electron and proton momenta and angles. In Fig. 2 we plot the E_m and P_m distributions for the forward electron angle C data at $Q^2 = 0.6$ GeV^2 as a solid line. The data have been cut with $|P_m| < 300$ MeV/c and $E_m < 80$ MeV. The scattering from p-shell and s-shell nucleons is clearly resolved into two peaks in E_m.

The dashed lines are the distributions calculated from a realistic Monte Carlo model[13] which includes radiative corrections, normalized to the same number of total events. The agreement is reasonable, especially in the tail region at large E_m where the cut is placed. The p-shell peak at $E_m \sim 20$ MeV appears to be slightly shifted and broadened relative to the Monte Carlo. Similar effects exist in the analysis of (e,p) elastic scattering from the hydrogen target, and are thought to originate in incorrect momentum and scattering angle reconstruction. The ongoing analysis of the spectrometer optics should improve the agreement with the Monte Carlo.

In Fig. 3, we show a comparison of experimental and Monte Carlo cross-sections for all the forward electron angle, $Q^2 = 0.6$ GeV^2 data, as a function of proton angle. The same P_m and E_m cuts have been applied. In the top

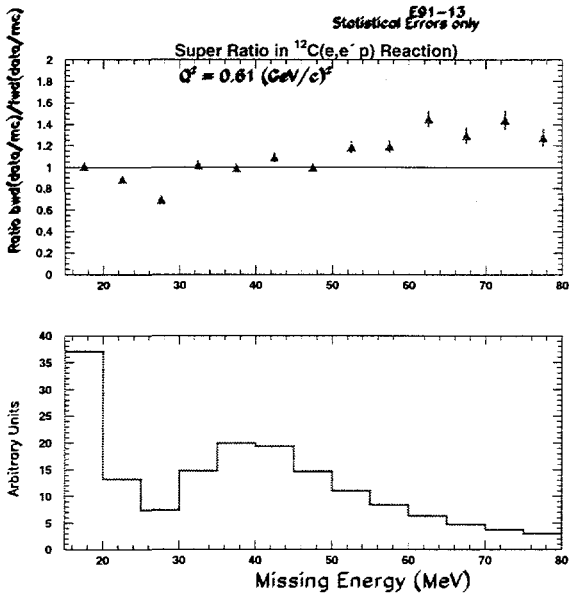

Figure 5: Ratio of $T_{\rm bwd}/T_{\rm fwd}$ versus E_m for the C data at $Q^2 = 0.6$ GeV^2. The E_m distribution is for the forward angle data is show in the lower panel.

panel we plot the ratio of the cross sections, and in the bottom panel we plot the yields, with the Monte Carlo normalized to the weighted average T of the corresponding data. All statistical uncertainties are smaller than the plotting symbols. One can see that there is essentially complete coverage of the proton angular distribution. The ratio of cross sections is fairly flat in the center, but rises at small and large proton angles. These angles correspond to large initial-state proton momenta that are underrepresented in the Monte Carlo (since the IPSM lacks the correlations from which they arise), leading to an increase in the ratio.

The weighted average T at each Q^2 is plotted versus $\sqrt{Q^2}$ in Fig. 4. A correction for the wave function correlations has been included. These preliminary results contain a 5% systematic uncertainty, which is dominated by the uncertainty with which we understand the spectrometer acceptances. The systematic uncertainties should decrease substantially after all the optics data have been analyzed. We can see that there is good agreement with the previous data. In addition, there appears to be a statistically significant difference between the backward and forward electron angle data at the same Q^2.

This backward/forward difference is illustrated in Fig. 5, in which we plot the ratio $T_{\rm bwd}/T_{\rm fwd}$ versus missing energy for the $Q^2 = 0.6$ GeV^2 carbon data. The backward angle data shows an enhancement relative to the forward angle data for $E_m > 50$ MeV. The full analysis of this data, including a Rosenbluth separation into longitudinal and transverse cross sections, is in progress.

Acknowledgments

We acknowledge the efforts of the TJNAF accelerator division in delivering high quality beam for this experiment. This work was supported in part by the U.S. Department of Energy, Nuclear Physics Division, under contract W-31-109-ENG-38, and by the National Science Foundation.

References

1. T. De Forest, *Nucl. Phys.* A **392**, 232 (1983).
2. T.G. O'Neill et al., *Phys. Lett.* B **351**, 87 (1995).
3. G. Garino et al., *Phys. Rev.* C **45**, 780 (1992).
4. T.G. O'Neill, California Institute of Technology Ph.D. thesis (1994).
5. G.R. Farrar et al., *Phys. Rev. Lett.* **61**, 686 (1988).
6. B.K. Jennings and G.A. Miller, *Phys. Rev.* D **44**, 692 (1991).
7. O. Benhar et al., *Phys. Rev. Lett.* **69**, 881 (1992).
8. L.L. Frankfurt et al., *Phys. Rev.* C **50**, 2189 (1994).
9. N.N. Nikolaev et al., *Nucl. Phys.* A **567**, 781 (1994).
10. A. Kohama, K. Yazaki, and R. Seki, *Nucl. Phys.* A **536**, 716 (1992).
11. A.S. Rinat and B.K. Jennings, *Nucl. Phys.* A **568**, 873 (1994).
12. W.A. Watson III et al., IEEE Trans. Nuc. Sci. **41**, 61.
13. N.C.R. Makins et al., *Phys. Rev. Lett.* **72**, 1986 (1994).